Polarization-Selective Out-Coupling of Whispering-Gallery Modes

Florian Sedlmeir,[1,2,*] Matthew R. Foreman,[1,3] Ulrich Vogl,[1,2] Richard Zeltner,[1,2] Gerhard Schunk,[1,2,4] Dmitry V. Strekalov,[1,2] Christoph Marquardt,[1,2] Gerd Leuchs,[1,2] and Harald G. L. Schwefel[5]

[1]*Max Planck Institute for the Science of Light, Staudtstraße 2, 91058 Erlangen, Germany*
[2]*Institute for Optics, Information and Photonics, University of Erlangen-Nürnberg, Staudtstraße 7/B2, 91058 Erlangen, Germany*
[3]*Department of Physics, Blackett Laboratory, Imperial College London, London SW7 2AZ, United Kingdom*
[4]*School of Advanced Optical Technologies (SAOT), University of Erlangen-Nürnberg, Paul-Gordan-Straße 6, 91052 Erlangen, Germany*
[5]*The Dodd-Walls Centre for Photonic and Quantum Technologies, Department of Physics, University of Otago, 730 Cumberland Street, Dunedin 9016, New Zealand*

(Received 5 September 2016; revised manuscript received 12 January 2017; published 27 February 2017)

Whispering-gallery mode (WGM) resonators are an important platform for linear, nonlinear, and quantum optical experiments. In such experiments, independent control of in-coupling and out-coupling rates to different modes can lead to higher conversion efficiencies and greater flexibility in the generation of nonclassical states based on parametric down-conversion. In this work, we introduce a scheme that enables selective out-coupling of WGMs belonging to a specific polarization family, while the orthogonally polarized modes remain largely unperturbed. Our technique utilizes material birefringence in both the resonator and the coupler such that a negative (positive) birefringence allows for polarization-selective coupling to TE (TM) WGMs. We formulate a refined coupling condition suitable for describing the case where the refractive indices of the resonator and the coupler are almost the same, from which we derive a criterion for polarization-selective coupling. Finally, we experimentally demonstrate our proposed method using a lithium niobate disk resonator coupled to a lithium niobate prism, where we show a 22-dB suppression of coupling to TM modes relative to TE modes.

DOI: 10.1103/PhysRevApplied.7.024029

I. INTRODUCTION

Convex-shaped dielectric resonators, such as spheroids and spheres, can support whispering-gallery modes (WGMs) by continuous total internal reflection of light at their surface. WGMs possess a number of unique properties which make them an outstanding platform for the study and exploitation of nonlinear optical effects [1,2]. First, since WGMs are guided by total internal reflection they are spatially well confined within the resonator. Together with extremely low losses, or, equivalently, high-quality (Q) factors, this leads to a strong intracavity field. Moreover, high-Q resonances can be supported over the complete spectral range for which the dielectric is transparent, enabling efficient all-resonant frequency mixing of vastly different wavelengths. For instance, conversion from microwave to optical frequencies [3,4] has recently been demonstrated. Further examples include second-harmonic generation (ranging from visible [5] to ultraviolet wavelengths [6]) and resonantly enhanced parametric down-conversion [7,8]. Octave-spanning frequency combs have also been realized with WGM resonators [9].

Two important metrics used to describe optical resonators are the rate at which photons couple into and out of the resonator (coupling rate) and the rate at which photons are absorbed or scattered inside the resonator (loss rate). Together, these rates determine the overall decay time within the resonator, the associated bandwidth of the mode, and the effective field enhancement (finesse) inside the resonator. While the loss rate is usually fixed, WGM resonators are commonly used with external dielectric couplers, such as tapered fibers [10] or prisms [11], which are placed within the evanescent field of the WGM such that it is partially converted to a propagating wave in the coupler (or vice versa). Evanescent coupling allows the coupling strength to be tuned continuously by adjusting the distance between the coupler and resonator. This represents one of the primary advantages of using a WGM system. Control of the coupling rates is desirable since it allows an optimal experimental regime to be reached. This regime is determined by the intrinsic losses and, in nonlinear experiments, by the nonlinear coupling coefficients. Specifically, in cavity-enhanced nonlinear optics experiments one usually tries to match the coupling rate to the sum of the loss rate and the nonlinear coupling rate between different modes [12]. As a result, the pump can be injected into the resonator, under the so-called critical coupling condition, with the highest efficiency

*Corresponding author.
florian.sedlmeir@mpl.mpg.de

possible. In WGM resonators, this can be realized, to some extent, by adjusting the evanescent coupling rate. In the usual configuration, however, the pump and the signal mode couple differently to a given prism due to their differing wavelengths (and hence evanescent decay length). Therefore, it is usually not possible to reach the ideal working regime in which both the pump mode and the signal modes are critically coupled. WGM crystalline resonators are also a versatile source of nonclassical light due to their excellent nonlinear properties [13]. Here, tunability of the coupling rate is also beneficial: optimal generation of squeezed light, either using parametric down-conversion or second-harmonic generation, requires a critically coupled pump beam to achieve maximum conversion efficiency, while the signal modes should be simultaneously overcoupled to minimize losses (decoherence) and hence preserve the fragile quantum states. If the resonator is used as a source of single photon pairs [14], overcoupling of the signal modes maximizes the heralding efficiency. Furthermore, tuning the coupling rate of the signal allows the bandwidth of the generated photon pairs to be adjusted to match atomic transitions [15]. All these applications ideally require the coupling rates of different modes to be independently tunable. Coupling light into WGMs (*in-coupling*) is highly selective since different modes often have different frequencies, different far-field properties, or different polarization. Selective excitation can thus often be achieved by tuning the laser frequency, adjusting the beam profile, or changing the state of polarization of the pump. If, however, different modes are simultaneously excited via nonlinear frequency conversion within the resonator, they can typically all couple out (*out-coupling*) through the same prism even if they have different properties. Decreasing the distance between the prism and the resonator causes all of the associated coupling rates to increase, and hence reduces the Q factor of all modes. Consequently, selective and independent manipulation of the individual coupling rates is not possible. Material birefringence, however, has been shown to facilitate polarization-selective coupling to modes of a dielectric ring resonator [16]. Specifically, if either the prism, the resonator, or both are birefringent, the effective refractive index experienced by TE and TM modes differs. If the effective refractive index experienced by a given polarization in the prism is below that of the resonator, out-coupling of the respective modes is suppressed. Accordingly, selective out-coupling of WGMs belonging to a single polarization family can be realized. In this article, we describe polarization-selective out-coupling using a prism and WGM resonator which are both fabricated from the same birefringent material. In this case, the refractive indices of the resonator and prism are comparable, although they may not be identical, depending on the orientation of their respective optic axes. For this system, we formulate the selective coupling criterion which allows us to establish which birefringent crystals are suitable for the realization of polarization-selective out-coupling. We find that the finite extent of the coupling region (or "coupling window") necessitates modification of the commonly used coupling condition [17]. Furthermore, we experimentally demonstrate selective out-coupling with a z-cut lithium niobate (LN) resonator (optic axis parallel to the symmetry axis) and an x-cut LN prism (optic axis perpendicular to that of the resonator). We find that out-coupling of TM modes is suppressed by 22 dB relative to that of highly overcoupled TE modes. With critically coupled TE modes, out-coupling of TM modes is not measurable.

II. THEORY

To first order, evanescent coupling of a WGM to a prism can be described using ray optics, whereby the WGM is treated as a plane wave propagating at a near-glancing angle to the resonator surface. The tangential component of the wave vector is equal to the propagation constant $\beta = k\overline{n}_r$ of the WGM, where k is the wave number in vacuum and $\overline{n}_r$ is the geometry-dependent effective refractive index of the mode [2]. Application of Snell's law then shows that the emission angle of the WGM into the prism is $\phi \approx \arcsin(\overline{n}_r/n_p)$, where n_p denotes the refractive index of the prism (see Fig. 1). Coupling can, therefore, only be achieved if $n_p \geq \overline{n}_r$. If this condition is not satisfied, only evanescent waves are formed in the prism and no energy is carried away from the resonator.

Closer examination of the coupling process reveals that the actual coupling condition is less strict than that given by geometric optics. Given that the resonator surface is curved and that the evanescent field outside the resonator decays quickly with distance, coupling occurs in a strongly localized region of space between the resonator and the coupler. This spatially confined field distribution can be described by an infinite sum of plane waves with their wave numbers distributed around the propagation constant β of the WGM. Consequently, even if the refractive index of the prism is slightly smaller than that of the resonator, coupling can still be achieved through a wing of this distribution.

In order to derive the coupling condition more quantitatively, we consider the WGM field distribution on the exterior surface of a disk-shaped resonator with major and minor radius of curvature R and r, respectively (see Fig. 1). The field on the surface of the resonator can be expressed as [18]

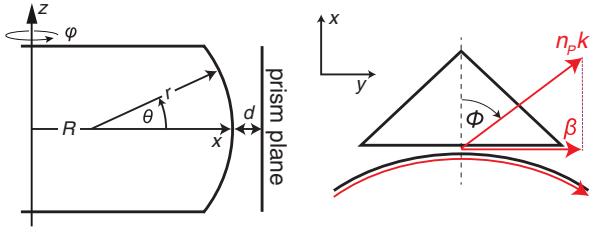

FIG. 1. (left) Coordinate system and geometrical parameters considered in this work. (right) Illustration of the coupling condition within the ray-optics picture.

$$\Psi^r(\theta,\varphi) \propto H_p\left[\frac{\theta}{\theta_m}\right]\exp\left[-\frac{\theta^2}{2\theta_m^2}\right]\exp[im\varphi], \quad (1)$$

where θ and φ are the polar and the azimuthal angles shown in Fig. 1, H_p are the pth-order Hermite polynomials, m and p are the azimuthal and polar mode numbers, and $\theta_m = (R/r)^{(3/4)}/\sqrt{m}$. Because of the evanescent nature of the mode outside the resonator, which can be well approximated by an exponential decay [19], the size of the coupling spot is small compared to the resonator size. We, therefore, can make the small-angle approximations $\theta \approx z/r$ and $\varphi \approx y/R$. The mode profile at the prism interface can, furthermore, be related to that at the resonator surface via $\Psi^p = T\Psi^r$, where

$$T(y,z) = \exp\left[-\kappa\left(d + \frac{z^2}{2r} + \frac{y^2}{2R}\right)\right] \quad (2)$$

describes the Gaussian coupling window [17]. The decay constant is given by $\kappa \approx k\sqrt{\overline{n}_r^2 - n_h^2}$, where n_h is the refractive index of the medium surrounding the resonator and d is the smallest distance between the prism and the resonator (see Fig. 1). While the y dependence of Ψ^p is thus ultimately determined only by the size of the coupling window and the angular momentum m of the WGM, the z behavior exhibits an additional dependence on the polar shape of the mode. The most commonly addressed WGM is the Gaussian-shaped fundamental mode ($p = 0$), for which $H_0 = 1$. In this case, the field in the plane of the coupling prism reduces to

$$\Psi^p(y,z) \propto \exp\left[-\frac{1}{2}\left(\frac{y^2}{\Delta y^2} + \frac{z^2}{\Delta z^2}\right)\right]\exp\left[i\beta y - \kappa d\right], \quad (3)$$

where $\Delta y^2 = R/\kappa$, $\Delta z^{-2} = (r\theta_m)^{-2} + (\kappa/r)^{-2}$, and the propagation constant is given by $\beta = m/R = k\overline{n}_r$. The field distribution at the prism surface can now be analytically decomposed into its Fourier components yielding [20]

$$\tilde{\Psi}^p(k_y,k_z) \propto \exp\left[-\frac{\Delta y^2}{2}(k_y-\beta)^2 + \frac{\Delta z^2}{2}k_z\right]. \quad (4)$$

The spatial Fourier components in the k_y direction are distributed around β with a spread of $\Delta k_y = 1/\Delta y$, whereas the k_z spectrum is centered on zero with a width of $\Delta k_z = 1/\Delta z$. Similarly to above, plane-wave components with $k_y^2 + k_z^2 \le n_p^2 k^2$ generate traveling waves upon transmission at the prism and therefore couple out of the resonator. Noting that $\Delta k_z \ll n_p k$, we can, however, safely neglect the k_z dependence. Designating a WGM to be coupled if $\beta - \Delta k_y \le n_p k$, we obtain the modified coupling condition

$$(\overline{n}_r - n_p)k \le \sqrt{\frac{\kappa}{R}} \quad \text{or} \quad \overline{n}_r - n_p \lesssim \sqrt{\frac{\sqrt{\overline{n}_r^2 - n_h^2}}{2\pi R/\lambda}}, \quad (5)$$

where we have used $k = 2\pi/\lambda$. To derive the second expression in Eq. (5), we have used the approximation of κ given above. Consequently, coupling is possible even if $\overline{n}_r > n_p$ due to the finite extent of the coupling window. Note that the effective refractive index $\overline{n}_r$ is always smaller than the bulk index of the resonator but approaches it for sufficiently large resonators. The deviation from the ray-optics coupling condition, where $\Delta k_y = 0$, becomes greater for smaller resonators and longer wavelengths since the corresponding smaller coupling window leads to a larger k spread.

Equation (5) also holds for the case of birefringent resonators and prisms. In this case, the polarization of the WGM determines the refractive index of the resonator and the prism. With a proper choice of material (i.e., magnitude of birefringence) and resonator size, selective coupling of WGMs belonging to a given polarization family can be achieved, while the orthogonally polarized modes remain uncoupled. Henceforth, we restrict attention to the case where both the resonator and prism are made from the same birefringent material, albeit with differently oriented optic axes. The basic configuration, shown in the inset of Fig. 2, is such that the optic axis of the resonator is aligned parallel to its symmetry axis (z cut), whereas the optic axis of the prism is normal to the coupling plane (x cut). Consequently,

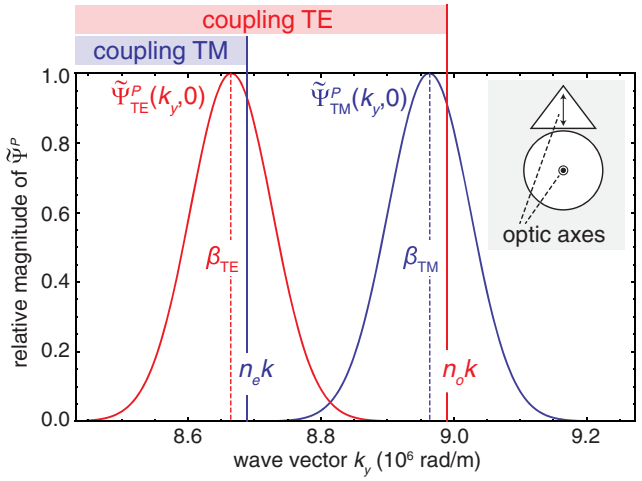

FIG. 2. The inset schematic shows the configuration considered in this work: the optic axis of the z-cut WGM resonator is perpendicular to the optic axis of the prism which are both made from the same material. The main plot shows the k_y spectrum of a fundamental TE and TM mode at the prism interface for the case of a LN resonator ($\lambda = 1550$ nm, $R = 2.1$ mm). The corresponding propagation constants and bulk wave numbers inside the LN prism ($n_o k$ and $n_e k$) are also indicated. Note that the coupling of the out-of-plane TE-polarized mode (red) is possible, whereas it is not for the in-plane TM case (blue).

TABLE I. Birefringent materials for which selective coupling using the scheme shown in Fig. 2 can be achieved. Note that the minimum resonator radius R_{min} required for selective coupling, as determined from Eq. (6), depends on wavelength (we assume $\lambda = 1550$ nm), birefringence ($\Delta n = n_o - n_e$), and the effective refractive index. The latter is calculated using the dispersion relation given in Ref. [18], assuming $r = R/7$.

Material	R_{min} (mm)	Δn	n_o	n_e
Lithium niobate [21]	0.24	−0.073	2.211	2.138
Barium borate [22]	0.09	−0.116	1.647	1.531
Lithium tetraborate [23]	0.31	−0.053	1.589	1.536
Rutile [24]	0.04	0.256	2.453	2.709
Crystal quartz [25]	8.41	0.008	1.528	1.536
Magnesium fluoride [26]	4.09	0.011	1.371	1.382
Sapphire [27]	9.85	−0.008	1.746	1.738

within the resonator the TE and TM modes experience the extraordinary (n_e) and ordinary (n_o) refractive index, respectively. In the prism the TE mode is ordinarily polarized and sees n_o. The TM mode is extraordinarily polarized and, therefore, each constituent plane wave has its own angle-dependent refractive index. Those waves propagating perpendicular to the optic axis, $k_x = 0$, experience a refractive index of n_e. Since this case corresponds to the transition from a propagating to an evanescent wave we take $n_p = n_e$ in Eq. (5) when considering TM modes. Selective coupling can thus be achieved with this arrangement for a negatively birefringent crystal when

$$[\overline{n}_r(n_o) - n_e]k > \sqrt{\frac{\kappa(n_o)}{R}}, \tag{6}$$

where we explicitly indicate the dependence of $\overline{n}_r$ on the ordinary refractive index. For a positive crystal, the ordinary and extraordinary refractive indices in Eq. (6) must be interchanged.

Table I lists a selection of birefringent resonator materials which can support high-Q WGMs and have been used, or have a potential use, in nonlinear optics. Also shown is the minimum resonator radius R_{min} required to achieve selective coupling of fundamental WGMs in a resonator in air, assuming an excitation wavelength of 1550 nm. A strong dependence of R_{min} on the magnitude of the birefringence $\Delta n = n_e - n_o$ is evident. A size limitation arises since for smaller resonators the coupling window narrows (broadening the corresponding angular spectrum) and geometrical dispersion reduces the effective refractive index $\overline{n}_r$. For shorter wavelengths the condition typically becomes less stringent due to decreased geometrical dispersion. Variation of R_{min} with the minor radius r is relatively weak. We note that Eq. (6) applies, in particular, to polarization-selective out-coupling of WGMs. Selective excitation (in-coupling) of modes with differing polarization can also be realized using an appropriately polarized pump beam. When the material birefringence is large, a proper choice of the in-coupling angle (when using prism coupling) can also lead to selective in-coupling.

III. EXPERIMENTAL DEMONSTRATION

In the remainder of this work, we present an experimental demonstration of polarization-selective out-coupling of a z-cut LN resonator to an x-cut LN prism. Since LN has a negative birefringence ($n_o > n_e$), TE modes can couple to the LN prism, whereas coupling of TM modes is suppressed. We note that the converse holds for a material with positive birefringence. For wavelengths $\lambda \approx 1550$ nm selective coupling is easily achieved for millimeter-sized LN resonators in air ($\Delta n = -0.073$, $\kappa \approx 8\ \mu\mathrm{m}^{-1}$), as further illustrated in Fig. 2, which shows the k_y Fourier spectra for fundamental TE and TM modes in a LN resonator with $R = 2.1$ mm and $r = 0.3$ mm. Practically, all Fourier components of the TE mode [$\tilde{\Psi}^p_{\mathrm{TE}}(k_y, 0)$, plotted in red] are smaller than the wave vector within the LN prism ($n_o k$) and, consequently, coupling is allowed. In contrast, all components of the TM mode [$\tilde{\Psi}^p_{\mathrm{TM}}(k_y, 0)$, plotted in blue] are larger than the associated wave vector in the LN prism ($n_e k$). In this case, no coupling can occur. Each Fourier spectrum is peaked at the respective propagation constant β, which, by virtue of the geometric dispersion of WGMs, is slightly smaller than the associated wave vector of a plane wave in a bulk crystal. This reflects the fact that the effective refractive index $\overline{n}_r$ is slightly smaller than the bulk index.

To experimentally demonstrate polarization-selective out-coupling, we use a two-port configuration composed of an isotropic (nonselective) in-coupling prism and an anisotropic (selective) out-coupling prism, as shown in Fig. 3(a). A diamond-turned z-cut LN resonator ($R = 2.1$ mm, $r = 0.3$ mm) is mounted onto a rotation stage. A narrow-band, frequency tunable telecom laser ($\lambda \approx 1550$ nm) is coupled into the resonator via a diamond prism after passing through a polarization controller. To determine the intrinsic loss rate of the resonator from the linewidths of the modes, the in-coupling prism is critically coupled to the WGM resonator. For the selective coupler we use a homemade x-cut LN prism. Both prisms are mounted on computer-controlled piezoelectric stages for precise distance control. The spectral positions and linewidths of excited modes are monitored in reflection after the in-coupling prism with a photodiode, as the LN prism is brought closer to the resonator. When light is coupled out of a given WGM through the LN prism, the linewidth and coupling depth of the mode are modified since the out-coupling acts as an additional loss channel. The prisms are mounted orthogonally to each other to prevent the LN prism from pushing the resonator towards the diamond prism, which would produce a change of the in-coupling rate, hence masking the effect of the out-coupler.

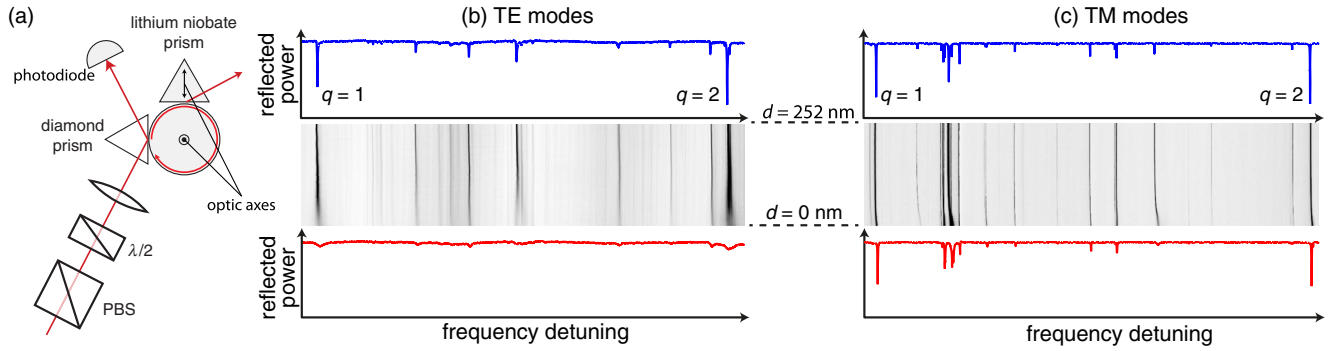

FIG. 3. (a) Schematic of the experimental setup. The gray intensity maps in panels (b) and (c) show the evolution of the spectra for the TE and TM modes, respectively, as the LN prism is brought closer to the resonator. The top (blue) spectra correspond to the critically coupled, almost unperturbed resonator (the distance between the LN prism and the resonator is approximately 252 nm), while the lower (red) plots show the spectra when the LN prism and resonator are in contact.

The uppermost (blue) plots in Figs. 3(a) and 3(c) show the observed TE- and TM-mode spectra under critical coupling conditions, when the LN prism is far from the resonator. Since the in-coupling angle required for excitation of TE and TM modes differs, the two polarizations are measured separately. We determine the radial mode order q via ordering the modes according to their free spectral range [28], whereas the $p = 0$ modes are identified by inspection of their relative coupling contrast [29]. The loaded linewidth of the fundamental TE (TM) mode is measured to be $\Delta\nu_{\mathrm{TE}} \approx 2.2$ MHz ($\Delta\nu_{\mathrm{TM}} \approx 1.0$ MHz) corresponding to a quality factor of $Q_{\mathrm{TE}} \approx 8.8 \times 10^7$ ($Q_{\mathrm{TM}} \approx 1.9 \times 10^8$). By increasing the voltage applied to the piezoelectric stage in increments of 0.1 V, the LN prism is slowly shifted towards the resonator in steps of approximately 6.3 nm (see below). For each step, the reflected spectra are recorded and are shown in the gray-scale intensity maps of Figs. 3(b) and 3(c). From top to bottom, the intensity map represents measured spectra as the separation between the LN prism and the resonator is varied from 252 to 0 nm. Both TE and TM modes remain unperturbed until the LN prism draws close to the resonator ($d \sim 1/\kappa$), where the modes start to shift in frequency due to the dielectric interaction with the LN prism [20]. The TE modes show significant linewidth broadening and become strongly undercoupled as shown in the lower spectrum of Fig. 3(c). In contrast, the TM modes show almost no linewidth change as expected.

For quantification, we select the two lowest radial-order modes ($q = 1, 2$) for both TE and TM polarizations and determine the associated resonance linewidths for every voltage step by means of Lorentzian fitting. The measured linewidths $\Delta\nu$ can be expressed as $\Delta\nu_c + \Delta\nu_i + \Delta\nu_c^{\mathrm{LN}}$, where $\Delta\nu_c$ represents the constant coupling rate to the diamond prism, $\Delta\nu_i$ denotes the intrinsic loss rate, and $\Delta\nu_c^{\mathrm{LN}}$ is the variable coupling rate to the LN prism. Subtraction of the unperturbed linewidth (measured when the LN prism is far from the resonator) from those determined as the LN prism is brought closer allows $\Delta\nu_c^{\mathrm{LN}}$ to be found. The experimentally determined coupling rates $\Delta\nu_c^{\mathrm{LN}}$ are plotted in Fig. 4 as a function of the relative voltage applied to the piezoelectric stage shifting the LN prism. An estimate of the distance traveled by the piezoelectric stage per volt can also be deduced from the variation of the TE coupling rate by noting that $\Delta\nu_c^{\mathrm{LN}} \propto e^{-2\kappa d}$, which yields a displacement of approximately 63 nm/V. We show the estimated separation between the LN prism and the resonator on the upper axis of Fig. 4. When plotted on a logarithmic scale, the coupling linewidth increases with a constant gradient as d is

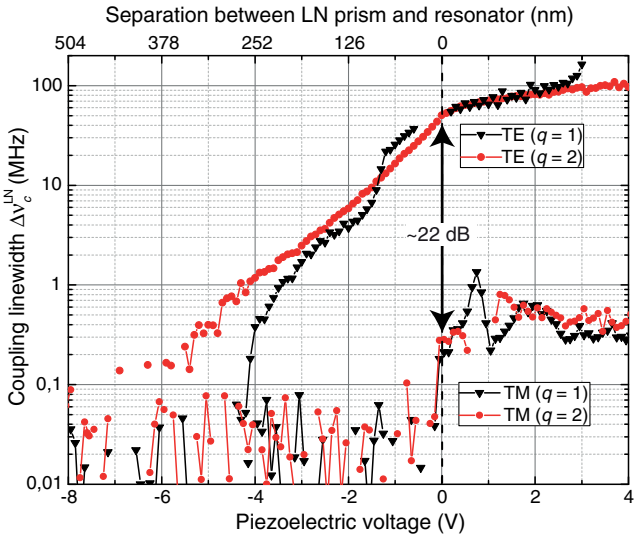

FIG. 4. WGM linewidth change induced by coupling to the LN prism for two different radial-order TE and TM modes. The linewidth changes are plotted against the voltage applied to the piezoelectric stage (bottom axis) and the corresponding estimated relative displacement of the LN prism (top axis). The qualitative change of the linewidths is used to identify the mechanical contact point between the LN prism and the resonator. The linewidth of the TE modes increases by approximately 53 MHz before contact, while the linewidth of the TM modes is largely unchanged.

decreased. The strong change in the gradient, seen in Fig. 4, is used to determine the position at which the LN prism and resonator come into mechanical contact. All voltages and distances have been defined relative to this point. At the contact point, the coupling rate of TE modes to the LN prism reaches 53 MHz, whereas the TM modes only weakly couple at a rate of 0.3 MHz. Out-coupling of the TM modes relative to the TE modes is therefore suppressed by a factor of 177, or equivalently about 22 dB. A further increase of the piezoelectric voltage pushes the LN prism into the resonator leading to further increases in the observed linewidths, attributable to deformation of the resonator and an associated higher intrinsic loss. The steplike increase in the TM linewidth upon contact is ascribed to these additional losses or alternatively to a slight modification of the distance between the in-coupling diamond prism and the resonator.

IV. CONCLUSION

In conclusion, we have derived a criterion for polarization-selective coupling using a prism and resonator of the same material. Many commonly used nonlinear crystals fulfill this condition. We have shown that an *x*-cut lithium niobate prism can be used to tune the rate at which TE modes of a *z*-cut LN resonator are out-coupled without disturbing the bandwidth of the TM modes. This provides a useful tool for nonlinear optical experiments in birefringent WGM resonators, allowing for independent control of coupling to differently polarized modes, which in many schemes correspond to the pump and the signal modes. We also provide a generalized coupling theory which accounts for the finite spatial extent of the coupling window. As a consequence, we find that coupling to WGMs is possible even if the refractive index of the prism is slightly smaller than the WGM effective index.

ACKNOWLEDGMENTS

D. V. S. acknowledges support from Alexander von Humboldt Foundation. G. L. is grateful for the financial support of the European Research Council under the Advanced Grant PACART.

F. S. and M. R. F. contributed equally to this paper.

[1] I. Breunig, Three-wave mixing in whispering gallery resonators, Laser Photonics Rev. **10**, 569 (2016).

[2] D. V. Strekalov, C. Marquardt, A. B. Matsko, H. G. L. Schwefel, and G. Leuchs, Nonlinear and quantum optics with whispering gallery resonators, J. Opt. **18**, 123002 (2016).

[3] V. S. Ilchenko, A. A. Savchenkov, A. B. Matsko, and L. Maleki, Whispering-gallery-mode electro-optic modulator and photonic microwave receiver, J. Opt. Soc. Am. B **20**, 333 (2003).

[4] A. Rueda, F. Sedlmeir, M. C. Collodo, U. Vogl, B. Stiller, G. Schunk, D. V. Strekalov, C. Marquardt, J. M. Fink, O. Painter, G. Leuchs, and H. G. L. Schwefel, Efficient microwave to optical photon conversion: An electro-optical realization, Optica **3**, 597 (2016).

[5] J. U. Fürst, D. V. Strekalov, D. Elser, M. Lassen, U. L. Andersen, C. Marquardt, and G. Leuchs, Naturally Phase-Matched Second-Harmonic Generation in a Whispering-Gallery-Mode Resonator, Phys. Rev. Lett. **104**, 153901 (2010).

[6] J. U. Fürst, K. Buse, I. Breunig, P. Becker, J. Liebertz, and L. Bohatý, Second-harmonic generation of light at 245 nm in a lithium tetraborate whispering gallery resonator, Opt. Lett. **40**, 1932 (2015).

[7] J. U. Fürst, D. V. Strekalov, D. Elser, A. Aiello, U. L. Andersen, C. Marquardt, and G. Leuchs, Low-Threshold Optical Parametric Oscillations in a Whispering Gallery Mode Resonator, Phys. Rev. Lett. **105**, 263904 (2010).

[8] C. S. Werner, T. Beckmann, K. Buse, and I. Breunig, Blue-pumped whispering gallery optical parametric oscillator, Opt. Lett. **37**, 4224 (2012).

[9] P. Del'Haye, T. Herr, E. Gavartin, M. L. Gorodetsky, R. Holzwarth, and T. J. Kippenberg, Octave Spanning Tunable Frequency Comb from a Microresonator, Phys. Rev. Lett. **107**, 063901 (2011).

[10] M. Cai, O. Painter, and K. J. Vahala, Observation of Critical Coupling in a Fiber Taper to a Silica-Microsphere Whispering-Gallery Mode System, Phys. Rev. Lett. **85**, 74 (2000).

[11] V. B. Braginsky, M. L. Gorodetsky, and V. S. Ilchenko, Quality-factor and nonlinear properties of optical whispering-gallery modes, Phys. Lett. A **137**, 393 (1989).

[12] B. Sturman and I. Breunig, Generic description of second-order nonlinear phenomena in whispering-gallery resonators, J. Opt. Soc. Am. B **28**, 2465 (2011).

[13] J. U. Fürst, D. V. Strekalov, D. Elser, A. Aiello, U. L. Andersen, C. Marquardt, and G. Leuchs, Quantum Light from a Whispering-Gallery-Mode Disk Resonator, Phys. Rev. Lett. **106**, 113901 (2011).

[14] M. Förtsch, J. Fürst, C. Wittmann, D. Strekalov, A. Aiello, M. V. Chekhova, C. Silberhorn, G. Leuchs, and C. Marquardt, A versatile source of single photons for quantum information processing, Nat. Commun. **4**, 1818 (2013).

[15] G. Schunk, U. Vogl, D. V. Strekalov, M. Förtsch, F. Sedlmeir, H. G. L. Schwefel, M. Göbelt, S. Christiansen, G. Leuchs, and C. Marquardt, Interfacing transitions of different alkali atoms and telecom bands using one narrowband photon pair source, Optica **2**, 773 (2015).

[16] K. Fiedler, S. Schiller, R. Paschotta, P. Kürz, and J. Mlynek, Highly efficient frequency doubling with a doubly resonant monolithic total-internal-reflection ring resonator, Opt. Lett. **18**, 1786 (1993).

[17] M. Gorodetsky and V. Ilchenko, High-*Q* optical whispering-gallery microresonators: Precession approach for spherical mode analysis and emission patterns with prism couplers, Opt. Commun. **113**, 133 (1994).

[18] I. Breunig, B. Sturman, F. Sedlmeir, H. G. L. Schwefel, and K. Buse, Whispering gallery modes at the rim of an axisymmetric optical resonator: Analytical versus numerical description and comparison with experiment, Opt. Express **21**, 30683 (2013).

[19] Y. A. Demchenko and M. L. Gorodetsky, Analytical estimates of eigenfrequencies, dispersion, and field distribution in whispering gallery resonators, J. Opt. Soc. Am. B **30**, 3056 (2013).

[20] M. R. Foreman, F. Sedlmeir, H. G. L. Schwefel, and G. Leuchs, Dielectric tuning and coupling of whispering gallery modes using an anisotropic prism, J. Opt. Soc. Am. B **33**, 2177 (2016).

[21] D. E. Zelmon, D. L. Small, and D. Jundt, Infrared corrected Sellmeier coefficients for congruently grown lithium niobate and 5 mol.% magnesium oxide-doped lithium niobate, J. Opt. Soc. Am. B **14**, 3319 (1997).

[22] D. Zhang, Y. Kong, and J.-Y. Zhang, Optical parametric properties of 532-nm-pumped beta-barium-borate near the infrared absorption edge, Opt. Commun. **184**, 485 (2000).

[23] T. Sugawara, R. Komatsu, and S. Uda, Linear and nonlinear optical properties of lithium tetraborate, Solid State Commun. **107**, 233 (1998).

[24] J. R. Devore, Refractive indices of rutile and sphalerite, J. Opt. Soc. Am. **41**, 416 (1951).

[25] G. Ghosh, Dispersion-equation coefficients for the refractive index and birefringence of calcite and quartz crystals, Opt. Commun. **163**, 95 (1999).

[26] M. J. Dodge, Refractive properties of magnesium fluoride, Appl. Opt. **23**, 1980 (1984).

[27] M. A. Jeppesen, Some optical, thermo-optical, and piezo-optical properties of synthetic sapphire, J. Opt. Soc. Am. **48**, 629 (1958).

[28] J. Li, H. Lee, K. Y. Yang, and K. J. Vahala, Sideband spectroscopy and dispersion measurement in microcavities, Opt. Express **20**, 26337 (2012).

[29] G. Schunk, J. U. Fürst, M. Förtsch, D. V. Strekalov, U. Vogl, F. Sedlmeir, H. G. L. Schwefel, G. Leuchs, and C. Marquardt, Identifying modes of large whispering-gallery mode resonators from the spectrum and emission pattern, Opt. Express **22**, 30795 (2014).